Synoptic Variability of Low-Cloud Properties and Meteorological Parameters in the Subtropical Trade Wind Boundary Layer

STEPHEN A. KLEIN

Program in Atmospheric and Oceanic Sciences, Princeton University, Princeton, New Jersey

ABSTRACT

Synoptic variability of low-cloud properties, temperature advection, and thermodynamic soundings of the trade wind boundary layer are analyzed, using the long data record from ocean weather station November (30°N, 140°W). The variations in low-cloud amount at this subtropical site are most strongly correlated with variations in temperature advection, the stability of the lower troposphere, and the relative humidity of the cloud layer. No single predictor is capable of explaining more than 13% of the variance in low-cloud amount. However, the amount of variance explained increases considerably when the data are averaged over several days. Four parameterizations for the amount of stratiform cloud under a subsidence inversion are tested against the observed amount of low clouds. The four parameterizations are based upon relative humidity, the inversion strength, a mixing line slope, and the amount of condensed water. All parameterizations are positively correlated with the observed cloud amounts, although the variance explained is less than 16%.

1. Introduction

Recent observational studies have shown that variations in monthly mean low-cloud amount are closely coupled to variations in monthly mean atmospheric circulation, monthly mean sea surface temperature (SST), and monthly mean stability of the lower troposphere, roughly defined as the difference in potential temperature between 700 mb and the surface (Hanson 1991; Peterson et al. 1992; Klein and Hartmann 1993; Oreopoulos and Davies 1993; Weare 1994; Norris and Leovy 1994; Klein et al. 1995; Fu et al. 1996). However, evidence for how well low cloudiness is tied to atmospheric circulation, sea surface temperature, or the stability of the lower troposphere at shorter timescales is lacking. If one were to use the stability of the lower troposphere to diagnose low-cloud amount, as has been done in some GCM simulations (Philander et al. 1996), one would hope that the parameterization would work not just for monthly mean variations, but for daily variations as well. In this paper, data from ocean weather station November (OWS N) are used to test how cloudiness and large-scale factors are related at timescales shorter than a month.

There are two primary timescales shorter than a month of interest: the diurnal cycle and synoptic variability. By synoptic variability, I mean variations in boundary layer properties occurring on timescales greater than one day but less than a month. Regarding the diurnal cycle in low-cloud amount, there is a maximum just before dawn and a minimum near 1500 LT (Minnis and Harrison 1984; Minnis et al. 1992; Heck et al. 1990; Rozendaal et al. 1995; and many more). The diurnal cycle in cloud shortwave absorption leads in the afternoon to a ''decoupling'' of the turbulent circulations in the cloud layer from those in the subcloud layer and a vertical thinning of the cloud (Nicholls 1984; Betts 1989). A decoupled boundary layer is one in which the turbulence in the upper half of the boundary layer is not well connected to the turbulence in the near-surface layer. Once a boundary layer has decoupled, moisture evaporated from the ocean surface accumulates in the near-surface layer and the usual flux of moisture from the surface to the cloud layer is reduced. Decoupling is thought to be important in determining both the diurnal cycle (Nicholls 1984) as well as the breakup of stratocumulus into trade cumulus (Krueger et al. 1995a,b; Bretherton and Wyant 1997; Wyant et al. 1997). Because diurnal variability has been well studied before, it is not discussed further in this paper.

Synoptic variability in marine stratocumulus has been studied much less frequently. Phenomena studied include coastal clearing episodes resulting from offshore flow events (Kloesel 1992) and the propagation of stratus/fog along the California coast due to coastal-trapped Kelvin waves, often associated with the ''Catalina eddy'' (Dorman 1985; Mass and Albright 1989; Leipper 1994; Rogerson and Samelson 1995). Synoptic variations in open-ocean low-cloud amount have been stud-

Corresponding author address: Stephen A. Klein, NOAA/Goddard Fluid Dynamics Laboratory, Princeton University, P.O. 308, Princeton, NJ 08542.
E-mail: sak@gfdl.gov

ied even more rarely. Wylie et al. (1989) studied synoptic variations in low-cloud amount during the First ISCCP Regional Experiment (FIRE) (Albrecht et al. 1988). They found that increases in low-cloud amount were statistically related to increases in cold advection, to increases in 500-mb height, and to decreases in boundary layer depth. Bretherton et al. (1995) analyzed synoptic variations in boundary layer cloud amount during the Atlantic Stratocumulus Transition Experiment (ASTEX) (Albrecht et al. 1995a) and found that low-cloud amount was consistently correlated with relative humidity in the upper half of the cloud layer and uncorrelated with other sounding parameters, including a stability index based on Klein and Hartmann (1993). However the sample size in these studies was quite small, consisting of only one month's variations in low-cloud amount.

Ocean weather station November was located approximately halfway between San Francisco and Hawaii at 30°N, 140°W and took routine meteorological observations including radiosonde data from 1949 until 1974. The climatology of this location was discussed extensively in Klein et al. (1995, hereafter KHN). During the oceanic summer season (June–September), this location lies in the steady trade wind circulation of the northeast Pacific. The typical environment at this location features a moist boundary layer beneath a relatively strong trade inversion. The boundary layer appears to be decoupled both during the day and night although the cloud amount is quite high. In addition to documenting the mean summertime climate, KHN studied the interannual variability in boundary layer properties and many of the results in that paper, which only used monthly mean data, will be compared with results in this paper. The long record of cloud variations at OWS N provides a unique opportunity to statistically evaluate the relationships between low-cloud amount and other meteorological parameters. From the 25 June to September periods of data from OWS N, there are 2374 days of simultaneous surface observations, cloud observations, and atmospheric soundings. To my knowledge, this represents the largest dataset of boundary layer variations ever studied.

The outline of the paper is as follows. Section 2 describes how the data were organized. Section 3 discusses the correlation of low-cloud amount with various sounding and surface variables. The following section presents both local sounding and surface variables and regional ship observations composited according to various categories of the recorded low-cloud amount at OWS N. Section 5 tests some of the typical parameterizations of marine stratocumulus in large-scale models against the available data from OWS N. Conclusions follow in section 6.

2. Data reduction and correlation analysis

a. OWS N sounding data

OWS N took standard surface meteorological observations every 3 h and launched radiosondes every 12

h between 1949 and 1974. To focus on synoptic variability during the season when the trade wind system is well developed at the location of N, I only considered data taken from the calendar months of June through September. Furthermore, due to instrumental error in the radiosonde daytime relative humidity data (see the appendix), I only considered radiosonde data taken at the 1200 UTC hour, approximately 0240 LT. [Prior to June 1, 1957 the nighttime sounding was taken at 1500 UTC (0550 LT).] The soundings reported values of temperature and relative humidity at the surface and every 50-mb level above and including 1000 mb. Due to a change in radiosonde instruments that occurred near the beginning of 1966, I have applied corrections to the pre-1966 data to make it more homogenous with the post-1966 data. In addition, all radiosonde humidities at levels higher than 1000 mb were multiplied by 1.05 to correct for insensitivities of the temperature of the hygristor strip. These two corrections and the rationale behind them are fully described in the appendix.

From the sounding data, several quantities can be calculated. First the pressure level of the trade inversion, p_{inv}, is estimated from the following algorithm, which takes advantage of the fact that the trade inversion is a layer typified by a rise in temperature with height and a drop in relative humidity with height. With each sounding the 50-mb layer with the least fall in temperature with height was identified from all the 50-mb layers between 500 and 1000 mb. In addition, the 50-mb layer with the greatest fall in relative humidity with height was identified from the same sounding. If the 50-mb layer with the least fall in temperature and the greatest drop in relative humidity with height were the same layer, then the base of the trade inversion was marked as the pressure at the base of this 50-mb layer. If the layer identified by temperature differs from the layer identified by relative humidity, the level of the trade inversion was defined to be missing.

From those soundings for which the trade inversion was identified, additional thermodynamic quantities were calculated. The typical climate at N includes cumulus clouds underneath horizontally extensive stratocumulus clouds that lie within the uppermost part of the boundary layer (KHN 1995). I have calculated an estimate to the relative humidity in the uppermost part of the boundary layer, which will be called "cloud level" relative humidity, RH_{cl}. In addition, RH_{cl} was defined as the relative humidity interpolated to a height 90% of the way from the surface to the trade inversion base. For example, if the surface pressure was 1020 mb and the base of the trade inversion was identified as 850 mb, RH_{cl} would be set equal to the value of relative humidity interpolated to 867 mb. The value of 90% was chosen to match that used by Albrecht et al. (1995b).

To ascertain the degree of well-mixedness in the boundary layer, the drop in equivalent potential temperature, $\delta\theta_e$, within the boundary layer was also computed. Here, $\delta\theta_e$ was defined as the θ_e interpolated to a

height 20% of the way from the surface to the trade inversion base minus the θ_e interpolated to a height 90% of the way from the surface to trade inversion base, $\delta\theta_e \equiv \theta_e(z/z_i = 0.2) - \theta_e(z/z_i = 0.9)$. For example, if the surface pressure was 1020 mb and the base of the trade inversion was identified as 850 mb, $\delta\theta_e$ would be set equal to the value of θ_e interpolated to 986 mb minus the value of θ_e interpolated to 867 mb. The value $\delta\theta_e$ can be thought of as an indicator of decoupling; for boundary layers that are well mixed $\delta\theta_e$ is zero, while for decoupled boundary layers $\delta\theta_e$ is typically a few degrees Celsius. The inversion normalized height of 0.2 generally corresponds to the subcloud layer and was chosen to match that used by Albrecht et al. (1995b). This height is hopefully out of the surface layer where there are steep gradients in quantities such as mixing ratio between the values at the sea surface and those in the subcloud layer.

b. OWS N surface data

I extracted the surface meteorological observation at exactly the same nominal hour as the sounding. The standard meteorological observation includes information on surface air temperature and relative humidity, wind speed and direction, sea level pressure, SST, and cloud information. From this information, I estimated the surface fluxes of sensible and latent heat and the surface wind stress using the bulk formulas. The values of exchange coefficients are taken as functions of wind speed and air minus sea virtual temperature difference from Tables 3 and 4 of Smith (1988). These tables assume that the wind data were taken at 20 m above the ocean surface and that the air temperature and humidity data were taken at 10 m above the ocean surface. Quayle (1980) suggests that the average height of the anemometer at U.S. OWSs was typically 25 m. Temperature advection at the time of each observation is estimated as the dot product of the vector wind with the monthly mean large-scale gradient in SST calculated from COADS (Comprehensive Ocean–Atmosphere Data Set) SST data (Woodruff et al. 1987). The large-scale gradient in SST was calculated for each calendar month from the COADS monthly mean SSTs in the vicinity of OWS N. This calculation of temperature advection is identical to that of KHN except that the instantaneous wind vector is used instead of the monthly mean wind vector. From the visually recorded cloud information I extracted the amount of sky covered by clouds at the lowest level (in octas). Those observations with adequate sky illumination were identified following the criterion of Hahn et al. (1995). Keeping track of the sky illumination is important since previous work with this dataset indicated that the amount of low cloud was underestimated by 5% on nights without adequate moonlight (Rozendaal et al. 1995).

In addition to extracting the surface meteorological observation at the nominal hour of the sounding, I extracted the data from the observation taken 3 h before and after the nominal hour of the sounding time. I then averaged all variables from surface data over these three observation times to produce a single number to match each individual sounding. Because the soundings were taken at 0240 LT (0540 LT before 1 June 1957), the surface quantities represent an average over the period 2340 LT–0540 LT (0240–0840 LT before 1 June 1957). Because cloud amount at OWS N for these hours is greater than at all other hours diurnally (Rozendaal et al. 1995), this nighttime period corresponds to one extreme of the diurnal cycle. Data when averaged this way will be referred to as ''nighttime'' data, for example ''nighttime low-cloud amount.''

There are two purposes for this averaging of surface data over the 3 h before and after the nominal hour of the sounding. The first is that mesoscale variations in boundary layer properties may bias instantaneous observations of low-cloud amount and other properties (Agee et al. 1973). Low-cloud amount tends to vary with horizontal scales of anywhere from 5 to 100 km. Given that the observer's visual range is probably of order 30–50 km in radius (Barrett and Grant 1979; Henderson-Sellers et al. 1987) (and perhaps less when low clouds are present), the instantaneous surface observation of low-cloud amount may be substantially lower or higher than the large area (100–250 km) averaged low-cloud amount. The effective area seen by an observer when low-cloud amount and other surface data are averaged over the 3 h before and after the sounding is for a typical boundary layer wind speed of 6 m s^{-1} approximately 130 km along wind ($=6$ h $\times$ 6 m s^{-1}) by 80 km across wind ($=2$ times the radius of observation). Thus, averaging surface data into 6-h averages smooths over these mesoscale variations in low-cloud amount (and other parameters).

The second purpose for averaging surface data into 6-h averages is that the probability density function of the key variable in this paper, low-cloud amount, has fewer ''modes'' when the data are averaged over 6 h (Fig. 1). At any given instant, the surface observer is most likely to record the sky cover as 8 octas, that is, solid overcast. The second mode at 2 octas or a low-cloud amount of 0.25 corresponds to broken skies and is clearly separated from the overcast mode. The condition of no low clouds is rarely observed. For nighttime low-cloud amount, there is a single mode and the distribution is more normal, albeit with notable negative skewness. This distribution of nighttime low-cloud amount might be better characterized by an exponential or gamma distribution. The shape of the probability density function of low-cloud amount is important since the standard linear correlation techniques that I apply in section 3 have problems with datasets that are more modal.

c. COADS data

In section 4, the large-scale fields of sea level pressure and surface winds are composited according to whether

Instantaneous Low Cloud Amount
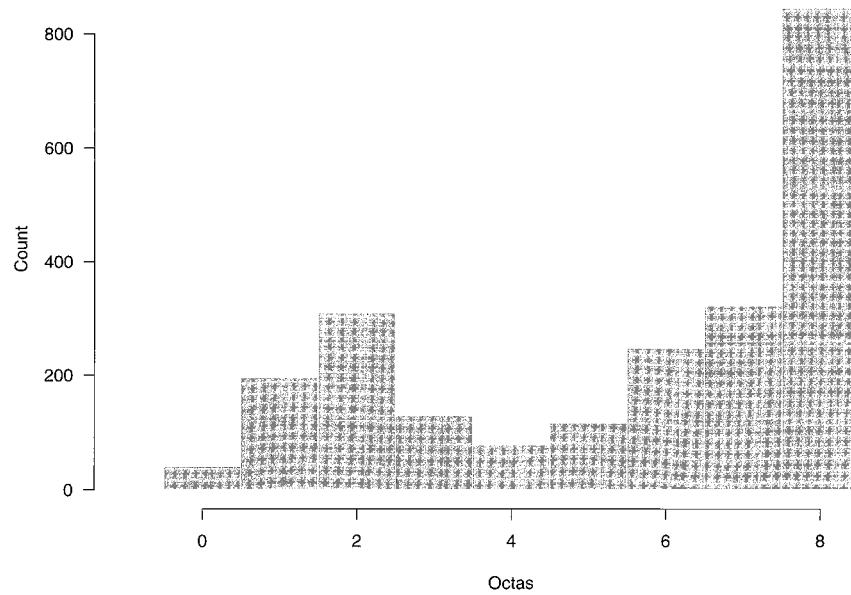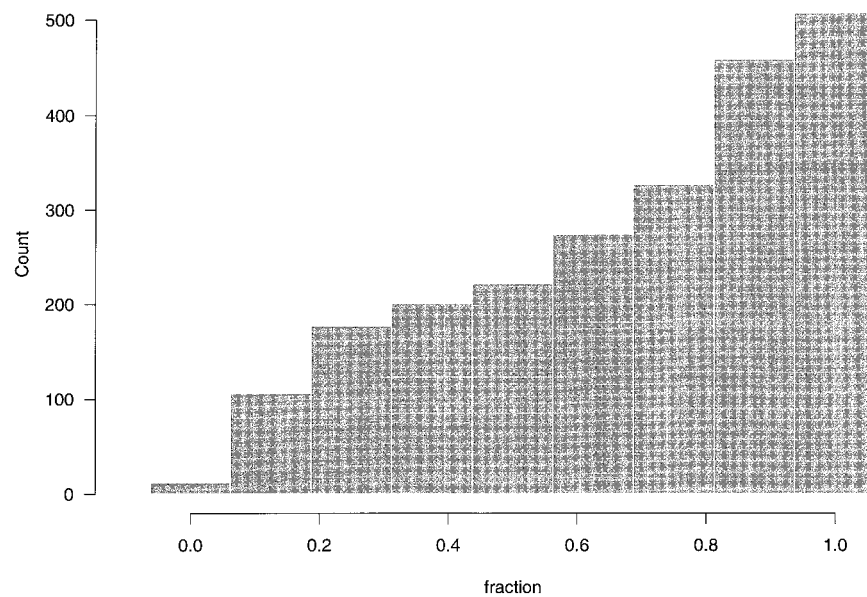

Nighttime Low Cloud Amount

FIG. 1. Histogram of June–September instantaneous (a) and nighttime (b) low-cloud amounts from ocean weather station November. The nighttime low-cloud amount results from averaging the low-cloud amount from an instantaneous observation with those of the surface report 3 h before and after the time of the instantaneous observation.

or not the nighttime low-cloud amount at OWS N falls within certain values. To composite the large-scale fields, I use the records of individual ship observations as compiled and quality controlled by COADS (Wood-

ruff et al. 1987). The ship observations used in this paper are those observations during the years 1954–74 from the Compressed Marine Reports and Long Marine Reports archives, which pass the quality control checks on
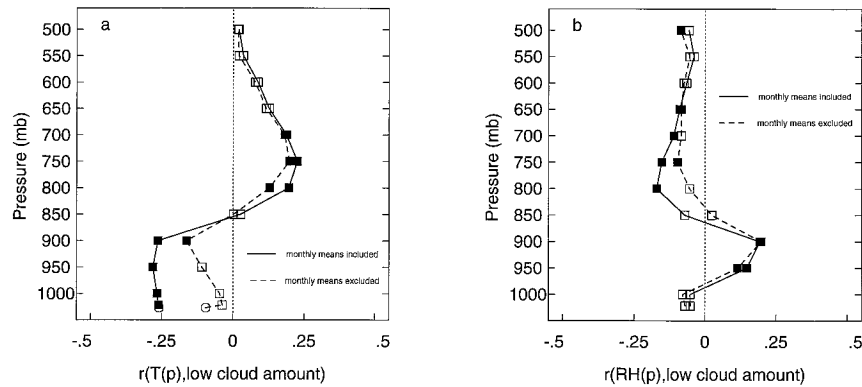
FIG. 2. Correlation coefficients between nighttime temperature (a) and nighttime relative humidity (b) at each level and nighttime low-cloud amount at N. In (a) the correlations between the nighttime SST and nighttime low-cloud amount are indicated by octagons. Correlations that are significant at the 99% level are indicated by blackened squares (or octagons for SST).

the cloud records performed by Hahn et al. (1996). The ship observations are composited on a 2° latitude–longitude grid.

d. Statistical methods

Because this dataset includes annual and interannual variability as well as daily variability, a second dataset was created. In this second dataset, the monthly mean value of each variable was subtracted from the original value to give a daily anomaly. Daily anomalies were only calculated for months with 10 or more daily observations. This second dataset presumably has variability only from timescales shorter than a month.

Because of autocorrelation within each time series, I need an estimate of the time between independent observations. For each variable the 1-day lag autocorrelation coefficient, r, was calculated and the time in days between independent observations, τ, was defined as $-2(\ln r)^{-1}$, following the method of Leith (1973). (If τ was less than 1 day or r less than zero, τ was set to 1 day.) Essentially, this formula assigns the time between independent observations for each variable to be twice the e-folding time of the autocorrelation function. From this method, τ for the nighttime low-cloud amount is 2.3 days, for temperature advection it is 6.4 days, and for the stability of the lower troposphere 6.1 days.

When assessing the significance of correlations between two variables (say variable x and y), the number of independent paired observations is required. This number is assigned to be the number of days covered by the paired x, y observations divided by the maximum of τ_x and τ_y. Significance is then determined using a standard t test given the value of the correlation coefficient, the number of independent paired observations, and a specified confidence level.

3. Correlation analysis

a. Correlations with the sounding variables

Figure 2 displays the correlation coefficient of temperature and relative humidity at each level with the nighttime low-cloud amount at N. The solid and dashed lines represent the dataset with and without monthly means included, respectively. This figure should be compared with interannual correlation of monthly mean temperatures and humidities with monthly mean low-cloud amount at N (Fig. 6 of KHN). Apart from the magnitudes of the correlation coefficients, the figures are remarkably similar, indicating that low-cloud amount is negatively correlated with temperatures beneath the trade inversion (~850 mb), positively correlated with temperatures immediately above the trade inversion, positively correlated with relative humidities in the cloud layer (~850–950 mb), and negatively correlated with relative humidities immediately above the trade inversion. Because increased subsidence would warm and dry the air, a coupling between increased subsidence and increased low-cloud amount may explain the correlations of above-inversion temperatures and relative humidities to low-cloud amount.

Comparing the correlation coefficients for the datasets with and without the monthly means included, it is apparent that much of the correlation between boundary layer (~900 mb to the surface) temperatures and low-cloud amount exists only on longer (i.e., monthly mean) timescales. This in part reflects the smaller day to day variance of boundary layer air temperatures. Another explanation for this feature may lie with the different response times of the SST and the boundary layer to a change in atmospheric circulation (KHN 1995). For example, consider the case that the strength of the subtropical high suddenly increased. As a result, low-cloud amount would increase in a matter of days. Accompanying this increase in low-cloud amount would be an

TABLE 1. Correlation coefficients between select local parameters and the nighttime low-cloud amount at *N*. Correlations not significant at the 99% level are in parentheses.

Parameter	Dataset including monthly means	Dataset including monthly means but only at times of good illumination	Dataset excluding monthly means
Temperature advection, $-\overline{\mathbf{V}}\cdot\nabla\overline{SST}$	−0.35	(−0.25)	−0.29
Stability of the lower troposphere, θ (750 mb) − θ_{sfc}	+0.35	+0.31	+0.22
RH_{cl}	+0.33	+0.33	+0.28
Surface wind speed	+0.27	(+0.16)	+0.24
Surface wind stress	+0.25	(+0.14)	+0.22
$\delta\theta_e$	−0.25	−0.22	−0.13
Latent heat flux	+0.22	(+0.12)	+0.23
Sea level pressure	+0.21	(+0.15)	(+0.09)
Sensible heat flux	+0.15	(+0.10)	(+0.09)
p_{inv}	+0.14	(+0.05)	(+0.03)

increase in the surface heat fluxes out of the ocean [mostly due to the increased wind speed (Ronca and Battisti 1997)] and a decrease in the radiative heat flux entering the ocean. [During the summer, the decrease in solar radiation entering the ocean exceeds the increase in longwave radiation entering the ocean (Table 2 of Norris and Leovy 1994).] Due to the substantial heat capacity of the ocean mixed layer, SSTs would not decrease until a few weeks after this increase in the strength of the subtropical high. Because of the close coupling of the boundary layer air temperatures to the SSTs, the boundary layer air temperatures would decrease a few weeks after this increase in the strength of the subtropical high. In this way, boundary layer temperatures and low-cloud amount would be correlated at the monthly mean timescales but not as well at the daily time scale.

Temperatures near 750 mb are generally above the trade inversion and thus are not as tightly coupled with the underlying SST as temperatures in the boundary layer are. Consequently temperatures at these levels change more frequently with the synoptic environment than boundary layer air temperatures do. For temperatures at these levels, the positive correlation with low-cloud amount is just as strong in the dataset without the monthly means as it is in the dataset with the monthly means. This is consistent with the upper-air temperatures having much shorter autocorrelation times and changing more rapidly than boundary layer air temperatures.

b. Correlations of other parameters with nighttime low-cloud amount at N

Table 1 presents the correlation coefficients of selected variables at N with the low-cloud amount at N. The most significant correlations of low-cloud amount with a large-scale factor are for the temperature advection and the stability of the lower troposphere. The sign of the correlation for temperature advection is such that greater cold advection leads to more cloud. When air blows from colder water (cold advection), the boundary layer is often heated and moistened from below. Consequently it is not surprising that the sensible and latent heat fluxes are positively correlated with the daily variations in low-cloud amount. That greater cold advection is associated with more clouds is consistent with the general experience of forecasters from the ASTEX experiment and with the results of Wylie et al. (1989) for FIRE data and Bretherton et al. (1995) for ASTEX data.

The structure of the temperature correlations in Fig. 2a suggests that low-cloud amount at N would also be correlated with the stability of the lower troposphere, here defined as the difference between the potential temperature of air at 750 mb and that of air at the surface. Indeed, similar to the seasonal and interannual variations (Klein and Hartmann 1993; KHN 1995), the stability of the lower troposphere is positively correlated with low-cloud amount on the daily timescale (Table 1). However, the magnitude of the correlation coefficient is substantially less than the correlation coefficients for seasonal or interannual variability, which are typically greater than 0.7. The relatively small correlation coefficient would explain why data that span short time periods (such as ASTEX data) may not have a statistically significant relationship between the stability of the lower troposphere and low-cloud amount (Bretherton et al. 1995).

With regard to other sounding variables, low-cloud amount at N is correlated with the relative humidity at the level of the cloud, RH_{cl}. This positive correlation is consistent with the results of Slingo (1980), Albrecht (1981), and Bretherton et al. (1995), who found a significant correlation between cloud amount and the relative humidity in the cloud layer for deep decoupled boundary layers. This correlation seems to reflect the fact that for a large-scale stratiform cloud to persist the relative humidity at the level of the cloud must be near 100%. The correlation of $\delta\theta_e$ with low-cloud amount at N is such that when the boundary layer is more well mixed, the cloud amount is higher than average. This agrees with the expectation that well-mixed boundary layers can more easily support marine stratocumulus, which typically have a higher cloud amounts.

Surface wind speed and surface wind stress are positively correlated with low-cloud amount. However, I note that the correlation coefficient between surface wind speed and temperature advection is -0.66 and the correlation coefficient between surface wind stress and temperature advection is -0.65. This suggests that the correlation of wind speed or stress with low-cloud amount is due in part to the fact that cases of increased wind speed or stress are cases of increased cold advection. Indeed, a previous study of interannual variability indicated that increased cold advection occurs when the subtropical high is stronger than average and the wind speeds in the boundary layer are high (KHN 1995; Klein 1994). Given this relationship on the interannual scale between temperature advection, cloud amount, and the strength of the subtropical high, it is not surprising to find that sea level pressure at the station is also positively correlated at the daily timescale with low-cloud amount at N.

The height of the trade inversion, p_{inv}, has a statistically significant correlation with the low-cloud amount at N, such that the trade inversion is lower in height (higher in pressure) when the low-cloud amount is greater than average. This matches the expectation that shallow boundary layers typically have marine stratocumulus with high values of the cloud amount whereas deep boundary layers typically have trade cumulus with lower values of the cloud amount. However, the correlation coefficient is smaller than those of temperature advection or the stability of the lower troposphere and for the dataset with the monthly means removed the correlation is statistically insignificant. The weakness of the correlation may be because the 50-mb vertical resolution of the sounding data is comparable to the standard deviation of p_{inv}, which is 47 mb.

Also included in Table 1 are the correlation coefficients that result when the nights without good illumination are removed from the dataset. The values of the correlation coefficients and their relative rank change somewhat; however, no correlation coefficient changes sign. The fact that fewer of the correlations are significant at the 99% level primarily results from the significantly fewer number of cloud observations made under conditions of good illumination (518 vs 2285). Apparently a large sample size is needed to significantly determine of the signs of these weak correlation coefficients.

Table 1 also displays the correlation coefficients that result when the monthly means are subtracted from the data. Comparing the correlation coefficients between the dataset with the monthly means included and the monthly mean removed, all variables keep the same sign to their correlation coefficient and most variables have a similar magnitude to their correlation coefficient. However, a few variables, such as the pressure of the trade inversion, the stability of the lower troposphere, and sea level pressure, lose over a third in the magnitude of their correlation coefficients.

Although most correlations are significant at the 99% level, the largest correlation coefficient has magnitude 0.35. Thus over 87% of the variance in nighttime low-cloud amount is unexplained by any single variable available for consideration in this dataset. Figure 3 displays scatterplots of four of the best predictors against low-cloud amount. (Note that although the instantaneous low-cloud amount is recorded in octas, because of averaging the nighttime low-cloud amount can take on one of 25 evenly spaced values between 0 and 1.) The smattering of points emphatically demonstrates the ineffectiveness of any single large-scale factor in predicting daily cloud amount variations.

c. Multilinear regression of predictors on low-cloud amount at N

It is somewhat disturbing that no single predictor can explain more than 13% of the variance in low-cloud amount. However, given that low-cloud amount is significantly correlated with many variables, a multiple regression might substantially increase the explained variance. Of course, the ability of a multiple regression to explain more variance than a single regression depends on choosing predictors that are reasonably independent of each other.

In picking predictors for low-cloud amount, I chose those predictors that might be considered "external" large-scale factors. The idea is that low-cloud amount responds to a variety of externally imposed forcings over which low-cloud amount in the short term (~days) does not control. For example, the sea level pressure and temperature advection reflect the large-scale synoptic environment and are not directly influenced by low-cloud amount. Additional external predictors include humidities and air temperatures above the trade inversion, SSTs, and the large-scale subsidence field (which is not available on the daily timescale). The internal temperature and moisture structure variables (e.g., RH_{cl} and $\delta\theta_e$) and the surface heat fluxes are not considered external predictors since feedbacks between the radiation and turbulence permit cloud processes in the short term to change the magnitudes of these variables.

For a multiple regression technique, a multilinear regression routine in the statistics/graphics program Splus was used. The routine adds and drops terms to the linear model based upon minimizing the sum of the deviance (proportional to the square of the residuals) and the number of predictors used in the model. Table 2 presents the fraction of variance in low-cloud amount explained by single and multiple regressions for three external predictors: temperature advection, the stability of the lower troposphere, and the water vapor mixing ratio of air at 750 mb [$w(750$ mb$)$]. Interestingly, the increase in explained variance by the multiple regression is small. No more than 20% of the variance in low-cloud amount is explainable by a multiple regression. One reason that
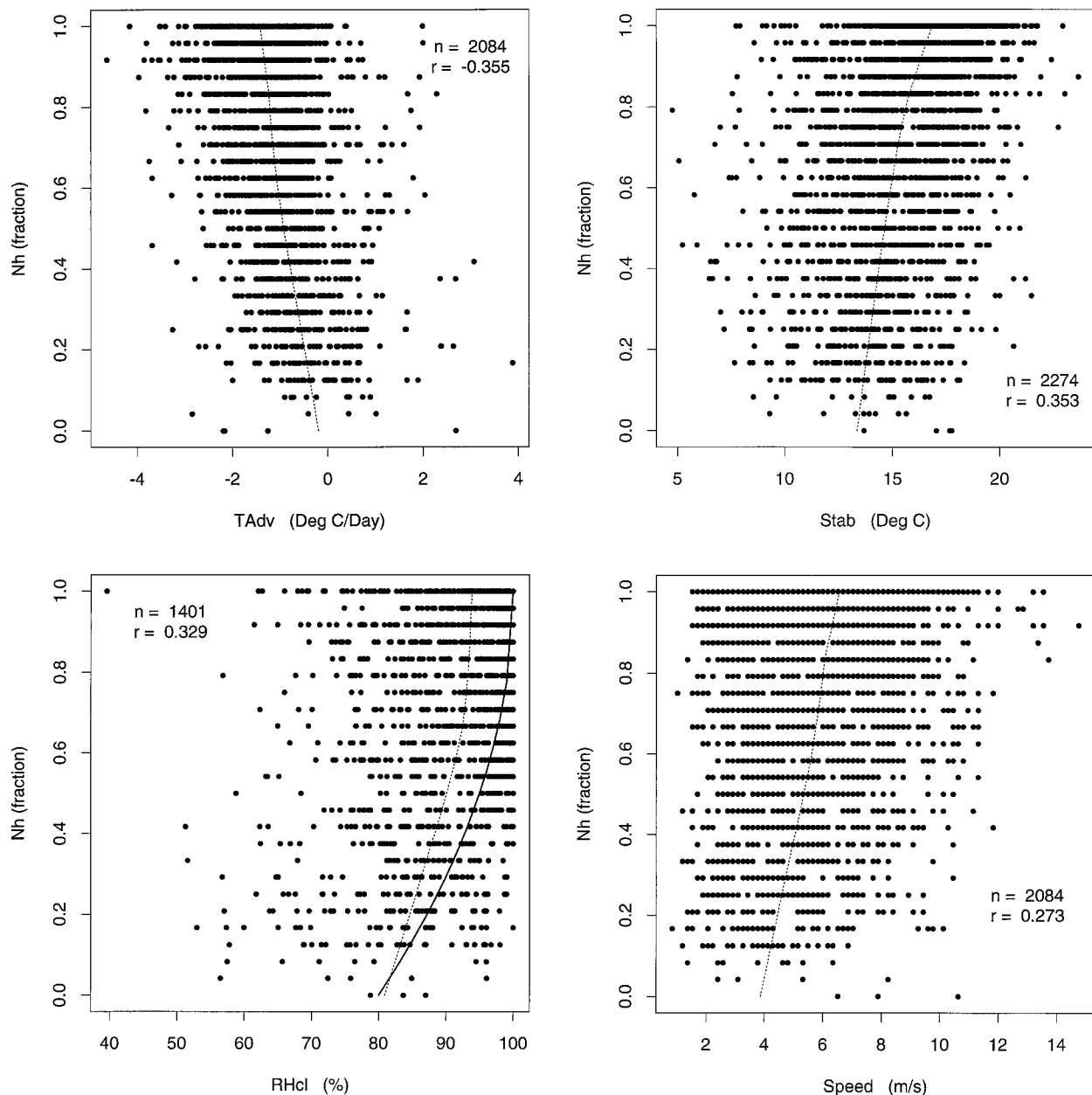
FIG. 3. Scatterplots of nighttime low-cloud amount ("Nh") against selected variables: Temperature advection (a), stability of the lower troposphere (b), relative humidity just beneath the trade inversion (c), and the surface wind speed (d). The thin dashed line in each figure is a smoothed curve fit to the data. (c) The heavy solid line is the parameterization of cloud amount as a function of relative humidity of Sundquist (1978). All correlations are significant at the 99% level.

the increase in explained variance is fairly small is that temperature advection and the stability of the lower troposphere are themselves correlated. Increased cold advection is associated with increased stability of the lower troposphere ($r = -0.33$). This association can plausibly be explained by the connection between a stronger subtropical high, increased cold advection at N, increased subsidence warming, and warmer temperatures aloft (KHN 95).

Modeling studies have shown that the amount of boundary layer cloud is sensitive to the moisture content of air above the trade inversion when all other external parameters are fixed. For example, Wang et al. (1993) indicated that an increase of moisture at 850 mb by 2 g kg^{-1} increased low-cloud amounts by 20%. From the data though, the water vapor mixing ratio of air at 750 mb explains less than 1% of the variance in cloud amount. Here, models and observations are in apparent disagreement; they can be reconciled by noting that humidity in nature may not vary alone without important

TABLE 2. Fraction of variance in nighttime low-cloud amount at N explained by various external predictors. For rows with a single predictor the fraction of variance explained is the square of the correlation coefficient. For rows with multiple predictors the fraction of variance explained is the square of the multiple correlation coefficient from a multilinear regression of cloud amount on the listed predictors.

Predictor	Dataset including monthly means	Dataset excluding monthly means
$-\overline{\mathbf{V}} \cdot \overline{\nabla SST}$	0.127	0.084
θ (750 mb) $- \theta_{sfc}$	0.118	0.048
w (750 mb)	0.008	0.003
$-\overline{\mathbf{V}} \cdot \overline{\nabla SST}$, θ (750 mb) $- \theta_{sfc}$	0.185	0.109
$-\overline{\mathbf{V}} \cdot \overline{\nabla SST}$, θ (750 mb) $- \theta_{sfc}$, w (750 mb)	0.186	0.110

changes in other external predictors (such as the subsidence rate or the radiation field), which can impact the cloud amount. Another possible reconciliation is related to the nature of the subsiding air. If the subsidence rate increases with height, subsidence will compress air masses of different origins such that the humidities of above inversion air located only a few tens of meters apart in the vertical may be dramatically different (Paluch et al. 1992). Since low-cloud amount can only respond to the humidity immediately above the cloud top (~850 mb), low-cloud amount may not be related to the humidity at 750 mb, a humidity that might be very different from that just above cloud top.

d. Lead/lag relationships

If the variations in the external parameters are to cause variations in low-cloud amount, it is tempting to look at lead/lag relationships for evidence of cause and effect. In particular, KHN presented evidence that at the interannual timescale variations in low-cloud amount at N are better related to variations in upwind SSTs, upwind above inversion temperatures, and upwind stabilities of the lower troposphere than to the local values of these parameters. They interpreted this correlation pattern as indicating that low-cloud amount responds to variations in the stability of the lower troposphere with a timescale of approximately 24–30 h.

Figure 4 presents the fraction of variance in low-cloud amount at various lead/lag times explained by the stability of the lower troposphere and its two components: the 750-mb temperature and the surface air temperature. Also shown are the fraction of variance in low-cloud amount explained by the SST and temperature advection. Low-cloud amount is best correlated with the simultaneous temperature advection indicating the rapid response of the boundary layer to the synoptic flow. Consistent with KHN (1995), low-cloud amount at N is best correlated with the stability of the lower troposphere from approximately 1 day earlier. This is due to a preferential correlation with 750-mb temperatures from approximately 1 day earlier. Somewhat surpris-
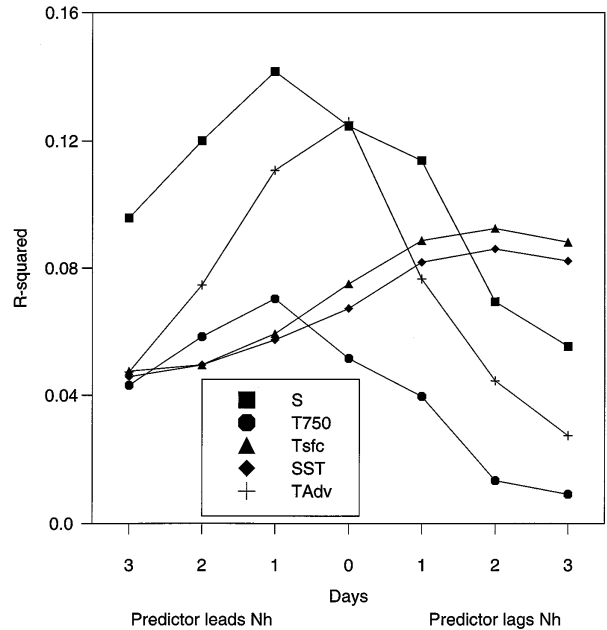

FIG. 4. Fraction of variance in nighttime low-cloud amount ("Nh") explained by the stability of the lower troposphere ("S"), the 750-mb temperature ("T750"), the surface air temperature ("Tsfc"), the sea surface temperature ("SST"), and the temperature advection ("TAdv") as a function of the lead/lag time. The dataset used was the full dataset including the monthly means. The stability of the lower troposphere and the temperature at 750 mb are positively correlated with low-cloud amount, while the surface air temperature, the sea surface temperature, and the temperature advection are negatively correlated with low-cloud amount.

ingly, low-cloud amount at N is better correlated with surface air temperatures and SSTs 1–2 days *later* than with simultaneous surface air temperatures and SSTs. This would seem to contradict the evidence from KHN that SST approximately 1 day upwind is a good predictor of low-cloud amount variations. In adition, a timescale of 1–2 days is much too short to be the response of the SST to increased cold advection, increased surface heat fluxes out of the ocean, and reduced radiation into the ocean from increased cloud cover (Ronca and Battisti 1997). A physical explanation for this result is unclear. It is worthwhile to note that none of the lead or lagged variance fractions are statistically different from the simultaneous variance fractions at the 99% confidence level.

e. Correlations as a function of the averaging interval

The amount of variance in low-cloud amount explained at the daily timescale is fairly low (~20%) when compared to the amount of variance in monthly averaged low-cloud amount that can be explained by external predictors (≥50%) (KHN; Klein and Hartmann 1993; Norris and Leovy 1994). It is interesting to ask at what timescale between 1 day and 1 month do external
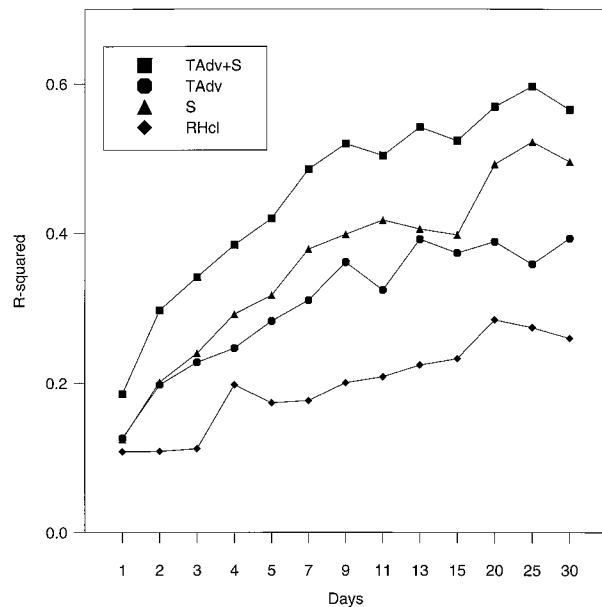
FIG. 5. Fraction of variance on nighttime low-cloud amount explained by various predictors as a function of the averaging interval. The predictors include temperature advection ("TAdv"), the stability of the lower troposphere ("S"), and the relative humidity of the cloud layer ("RHcl"). For lines with a single predictor the fraction of variance explained is the square of the correlation coefficient. For the line with multiple predictors the fraction of variance explained is the square of the multiple correlation coefficient from a multilinear regression of cloud amount on the listed predictors.

predictors become effective in explaining variations in low-cloud amount. Figure 5 displays the fraction of variance in low-cloud amount explained by three single predictors and one set of multiple predictors, as a function of the averaging interval. That is, the numbers plotted at 4 days correspond to the square of the correlation coefficients between 4-day mean low-cloud amounts and the simultaneous 4-day mean predictor(s).

There is no single averaging interval for which the variance explained rises dramatically from the previous averaging interval; instead the transition from 1-day to 30-day intervals in the variance explained is gradual, although by about 10 days the fraction of variance explained reaches most of the variance explained in monthly mean data. Thus if boundary layer clouds are parameterized using any of the effective predictors (i.e., the stability of the lower troposphere, temperature advection, or relative humidity of the cloud layer), the effectiveness of the parameterization increases with the averaging time interval such that cloud amount fluctuations with periods greater than 10 days are well parameterized (if "well parameterized" is defined by the fraction of explained variance exceeding 50%).

4. Compositing

The linear techniques used in the previous section make an assumption that the underlying distribution

of variables is fairly "normal" or Gaussian. However, Fig. 1b shows that the distribution of nighttime low-cloud amount is not very Gaussian, instead it is more like an exponential distribution. Consequently, methods such as linear correlation and regression may not be very effective. An alternative method to analyzing low-cloud amount variations that does not make assumptions about the frequency distribution of variables is compositing. For example, one can compare the composited values of sounding and surface properties for days when the nighttime low-cloud amount is small versus days when the nighttime low-cloud amount is large. In this section, the local sounding and surface variables as well as the regional ship observations from COADS will be composited according to categories of low-cloud amount.

Each day in the record of N was classified as having small, moderate, or large low-cloud amount. The values of low-cloud amount that separate the categories were chosen such that an ample number of days would fall in each category. With the boundary between small and moderate nighttime low-cloud amount set at 0.55 and the boundary between moderate and large nighttime low-cloud amount set at 0.9, the number of composited soundings in the small, moderate, and large low-cloud amount categories is 718, 865, and 702, respectively. Once all the days for each category have been determined, all the soundings and surface properties on the days for each category are linearly averaged (i.e., composited). Standard deviations and 99% confidence intervals for the means are saved. To determine a confidence interval, the number of independent observations is required. This is specified to be the number of days covered by the averaged observations divided by the time between independent observations (section 2d).

a. Compositing local sounding and surface quantities

Each category's sounding was formed by averaging the individual soundings on a scale of height relative to the trade inversion base and then the vertical axis was rescaled by the mean height of the trade inversion for that category (as in Albrecht et al. 1995b or KHN 1995). The composited soundings of potential temperature, relative humidity, water vapor mixing ratio, and equivalent potential temperature for each category are displayed in Fig. 6, and the composited values of selected variables are presented in Table 3. The trends in these soundings can be compared with the trends in the composite soundings from several field experiments presented by Albrecht et al. (1995b).

From the potential temperature soundings, it is clear that greater low-cloud amount is associated with increased stability of the lower troposphere, both because the boundary layer is cooler and because the air above the trade inversion is warmer. It is also apparent that the greater the low-cloud amount the
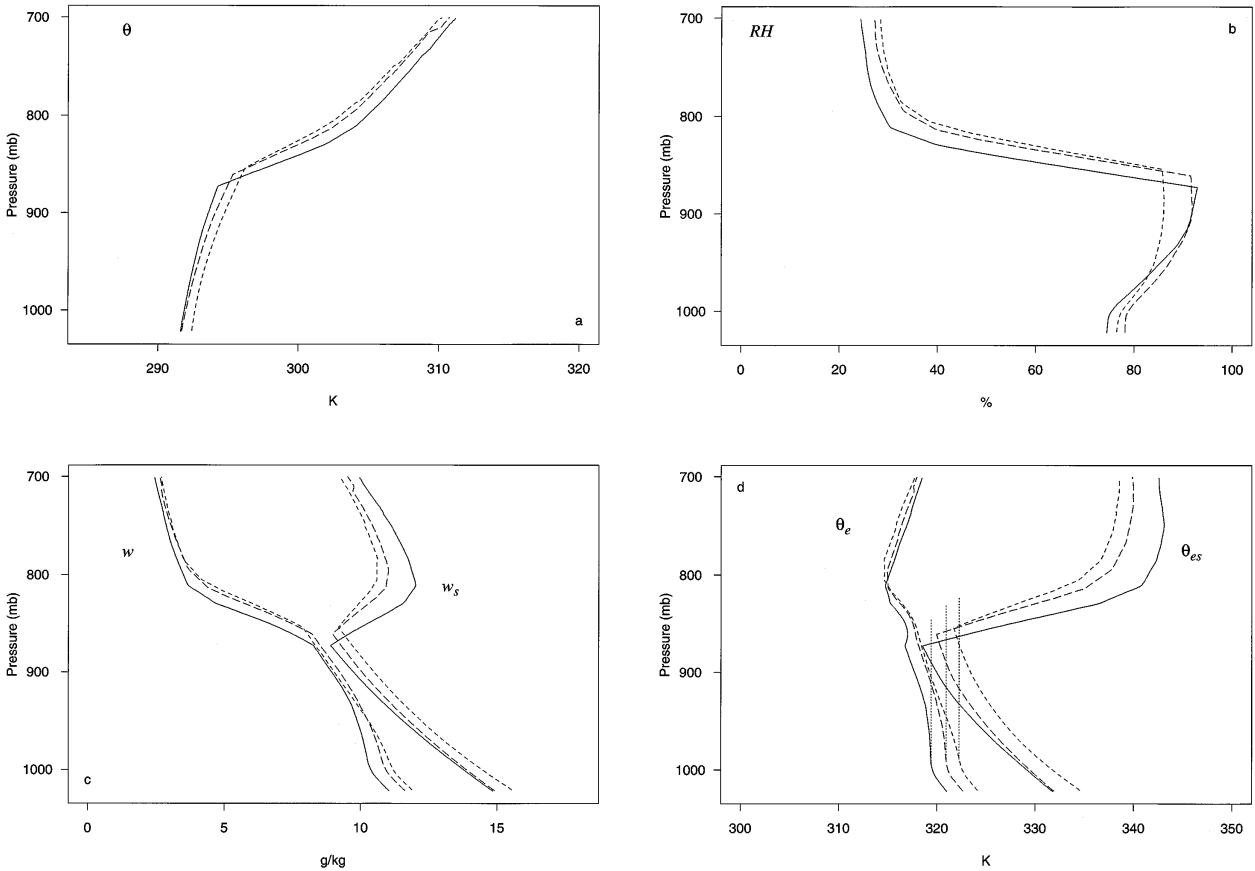
FIG. 6. Inversion-normalized soundings composited relative to nighttime low-cloud amount of (a) potential temperature, (b) relative humidity, (c) specific humidity and saturation specific humidity, and (d) equivalent potential temperature and saturation equivalent potential temperature. The vertical lines in (d) indicate the θ_e at an inversion normalized height of 0.2, and the difference of this line with θ_e's in the cloud layer is a measure of the convective available potential energy of the boundary layer. In each panel the sounding for cases of cloud amount less than 0.55 is indicated by the short dashed line, the sounding for cases of cloud amount greater than or equal to 0.55 and less than 0.90 is indicated by long dashed lines, and the sounding for cases of cloud amount greater than or equal to 0.90 is indicated by the solid line.

TABLE 3. Means and 99% confidence limits for selected variables classified according to categories of nighttime low-cloud amount.

Parameter	$N_h < 0.55$	$0.55 \leq N_h < 0.90$	$0.90 \leq N_h < 1.0$
Number of cases	718	865	702
N_h	0.34 ± 0.02	0.74 ± 0.01	0.97 ± 0.01
$-\overline{\mathbf{V}} \cdot \nabla \overline{SST}$ (°C day^{-1})	-0.65 ± 0.24	-1.17 ± 0.20	-1.40 ± 0.20
θ (750 mb) $- \theta_{sfc}$ (°C)	14.1 ± 0.7	15.3 ± 0.6	16.4 ± 0.6
RH$_{cl}$ (%)	85.9 ± 1.4	91.7 ± 0.9	92.3 ± 1.1
$\delta\theta_e$ (°C)	3.8 ± 0.4	2.6 ± 0.4	2.1 ± 0.4
Surface wind speed (m s^{-1})	5.0 ± 0.4	6.0 ± 0.4	6.5 ± 0.5
Surface wind stress (N m^{-2} × 100)	4.0 ± 0.7	5.8 ± 0.8	6.8 ± 1.0
Sensible heat flux (W m^{-2})	7.7 ± 1.5	10.3 ± 1.6	10.0 ± 1.8
Latent heat flux (W m^{-2})	92 ± 10	106 ± 9	119 ± 11
Sea level pressure (mb)	1021.4 ± 0.9	1022.3 ± 0.8	1022.9 ± 0.9
p_{inv} (mb)	854 ± 13	861 ± 9	873 ± 10
$\underline{SST}$ (°C)	22.4 ± 0.9	21.8 ± 0.8	21.6 ± 0.8
$\nabla \cdot \overline{\mathbf{V}}$ (10^{-6} s^{-1})	1.6	1.8	2.1
Lapse rate at an inversion normalized height of 0.9 (°C/km)	6.5	6.5	7.3
Lapse rate at an inversion normalized height of 0.9 divided by the moist adiabatic lapse rate	1.4	1.4	1.6

stronger the temperature inversion as measured by the magnitude of the jump in potential temperature at the top of the boundary layer. Near the boundary layer top, the lapse rates are between 6.5 and 7.3 K/km (Table 3). These lapse rates are conditionally unstable and quite comparable with lapse rates shown for the ASTEX composite soundings in Albrecht et al. (1995b). The presence of conditional instability is consistent with the dominant cloud type at OWS N, shallow cumulus underneath stratocumulus.

With regard to the humidity structure, the relative humidity near the top of the boundary layer increases with the amount of low cloud. Since large-scale stratiform clouds lie near the top of the boundary layer, the increase in relative humidity is consistent with the increase in cloud amount. Note that the cloud layer relative humidity for the nearly overcast category only reaches 92.3%. Given the reported cloud amount of 0.97 for this category and the assumption that the cloudy portion of the sky is saturated, the lowest physically possible relative humidity would be 97%. This suggests that even after the corrections applied to the relative humidity data (see the appendix) that the humidity data remained biased low. As discussed in the appendix, the poor original resolution of the data may contribute 2%–3% of the difference between 92.3% and 100% but cannot alone explain the undersaturation in the upper part of the boundary layer.

Figure 7d portrays the vertical profiles of θ_e and θ_{es} for each category of low-cloud amount. With regard to θ_e, Fig. 7d indicates that within the boundary layer all categories are not well mixed. The tabulated values of the θ_e drop within the boundary layer, $\delta\theta_e$, vary between 2° and 4°C and decrease as low-cloud amount increases (Table 3). That $\delta\theta_e$ is greater than zero for the nearly overcast category indicates that overcast conditions in a subtropical boundary layer need not be well mixed. The dashed vertical lines in Fig. 7d show that if an air parcel with properties at an inversion normalized height of 0.2 was raised to the upper part of the boundary layer, it would be buoyant for all categories.

With regard to some of the tabulated surface quantities, it is apparent that more overcast conditions are associated with more cold advection, greater surface wind speeds, and greater surface heat fluxes. These trends are consistent with those found from the correlation analysis. Also apparent from Table 3 and the soundings is that conditions of more cloud amount tend to occur with a shallower boundary layer. This likely results from the increased subsidence associated with conditions of greater cloud amount (see next section).

b. Compositing of regional ship observations

To provide the regional context for the composites discussed in the previous section, the individual ship observations of COADS can be composited according
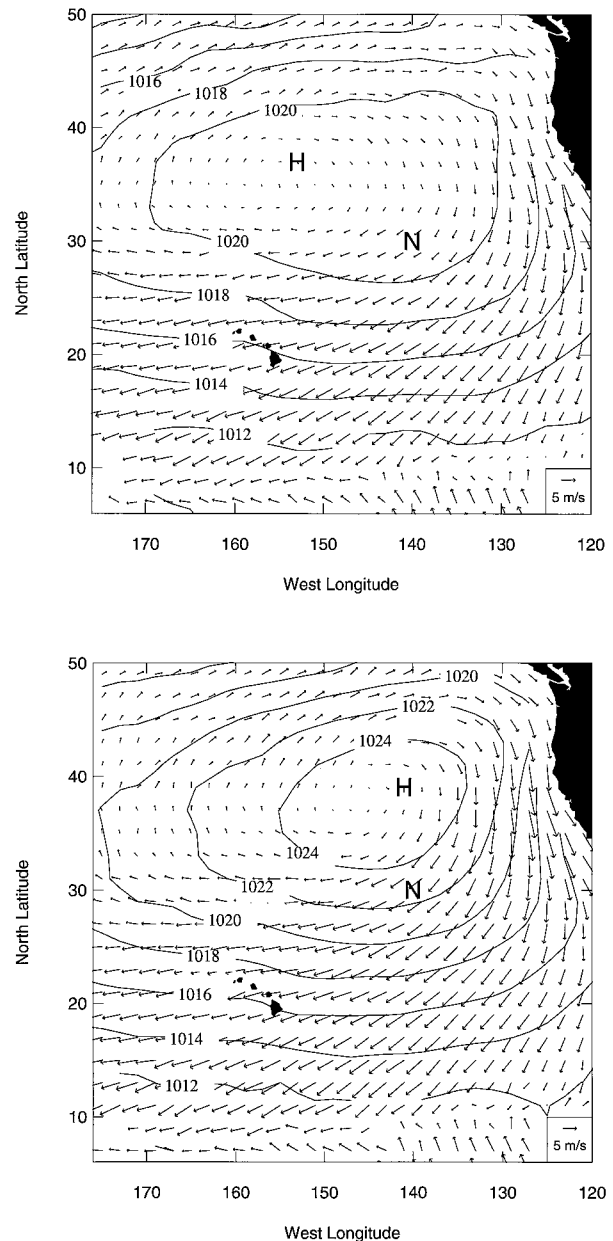

Fig. 7. Composite fields of COADS sea level pressure and surface winds (a) on days when the nighttime low-cloud amount at OWS N was less than 0.55 and (b) on days when the nighttime low-cloud amount at OWS N was greater than or equal to 0.90. The location of OWS N is indicated by the large letter "N" on the figures. The sea level pressure field is contoured with a contour interval of 2 mb. The large letter "H" indicates the location of the maximum value of sea level pressure.

to the same categories of cloud amount. That is, one can compute maps of average sea level pressure and surface winds on those days that the nighttime cloud amount at OWS N was less than 0.55, between 0.55 and 0.90, and above 0.90. A 2° latitude–longitude grid was established for the northeast Pacific, and the data from all the ship observations that occurred during the
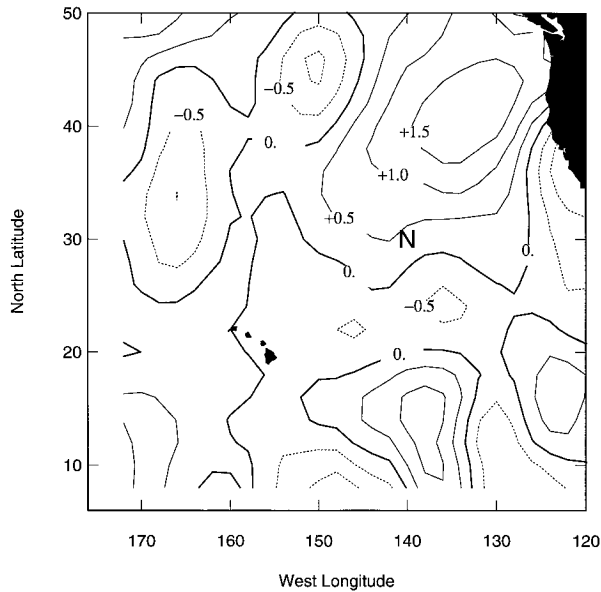
FIG. 8. The difference between the divergence of the surface wind in Fig. 7a and the divergence of the surface wind in Fig. 7b (Fig. 7b minus Fig. 7a). The contour interval is 0.5×10^{-6} s^{-1}.

list of days for a given category were linearly averaged. To qualify for compositing, the difference in time between the COADS ship observation and the OWS N observation had to be less than or equal to 12 h. For those grid boxes with fewer than 10 observations, a missing value code was inserted. The sea level pressure data has been smoothed by the application of a 1–2–1 filter in both the latitude and longitude directions. The wind data has not been smoothed.

Figure 7 displays the ship-observed fields of sea level pressure and surface winds for the days when the nighttime cloud amount at OWS N was less than 0.55 and the days when the nighttime cloud amount at OWS N was greater than or equal to 0.90. The figure for the intermediate category (which is not shown) lies in between the two figures. Clearly days of greater cloud amount at N are associated with a stronger subtropical high. The high is stronger both in terms of the peak sea level pressure and in terms of the compactness of the isobars. With a stronger high, the winds on the east side of the high are stronger and the trade wind flow near N is increased. From both wind fields one can compute the divergence of the surface wind field to get a measure of the subsidence rate. As for the sea level pressure data, the divergence field is smoothed by the same 1–2–1 filter. The difference in the surface wind divergence of these two wind fields is shown in Fig. 8 (large cloud amount category minus small cloud amount category). At N, the surface wind divergence increases with cloud amount (Fig. 8 and Table 3). Furthermore, Fig. 8 indicates increased subsidence to the north and east of the station and upwind in the mean flow. The increase in subsidence at and upwind from N is the likely cause for

the shallower boundary layer at N under conditions of increased cloud amount.

5. Evaluation of parameterizations of boundary layer cloud amount

The long record of OWS N permits one to test some of the commonly used or proposed parameterizations of boundary layer cloud amount for large-scale models. In particular, I test parameterizations based on four predictors: relative humidity, the inversion strength, the Betts–Boers mixing line slope (Betts and Boers 1990), and the amount of condensed water in clouds (Albrecht 1981).

a. Relative humidity parameterizations

Relative humidity in the upper part of the boundary layer where the stratiform cloud usually exists is among the top three predictors of nighttime low-cloud amount at N (Table 1). Thus one might expect that relative humidity would be a good variable to parameterize low-cloud amount with. How do actual parameterizations of low-cloud amount with relative humidity compare with the data in Fig. 3c? Figure 3c has two lines on it; the dashed line indicates the smooth curve fit to the data, whereas the heavy solid line indicates the parameterization of Sundquist (1978), where cloud amount, N, is parameterized as

$$N = \frac{\sqrt{100 - \mathrm{RH}_0} - \sqrt{100 - \mathrm{RH}}}{\sqrt{100 - \mathrm{RH}_0}}, \qquad (1)$$

where RH is the relative humidity in percent and RH_0 is a threshold relative humidity, here set to 80%, beneath which clouds do not occur. The parameterization predicts a sharp rise in cloud amount as relative humidity approaches 100% and furthermore the slope of cloud amount on relative humidity increases with relative humidity. The smooth curve fit to the data does not reach 100% relative humidity at a cloud amount of 1; however, this probably reflects errors in the relative humidity data rather than a true physical phenomenon. The smooth curve does have the property that the slope increases with relative humidity.

b. Inversion strength parameterizations

Slingo (1980, 1987) parameterized low-cloud amount according to the strength of the temperature inversion at the top of the boundary layer. In Slingo (1980) the amount is given by

$$N = -16.67(\Delta\theta/\Delta p)_{\min} - 1.167,$$

$$\text{for } -0.13 \le (\Delta\theta/\Delta p)_{\min} \le -0.07, \quad (2)$$

where $(\Delta\theta/\Delta p)_{\min}$ is the jump in potential temperature divided by the jump in pressure for the most stable layer in the lower troposphere. For $(\Delta\theta/\Delta p)_{\min} > -0.07$, N
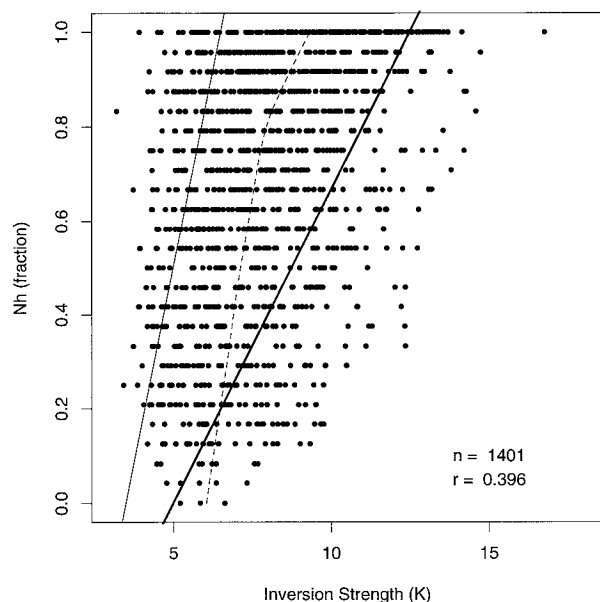
FIG. 9. Scatterplot of inversion strength against observed Nh. The thin dashed line is the smoothed curve fit to the data. The thin solid line is the parameterization of Slingo (1980) and the heavy solid line is the parameterization of Slingo (1987).

= 0, and for $(\Delta\theta/\Delta p)_{min} < -0.13$, $N = 1$. This parameterization was used in the U.K. Meteorological Office's 11-level model. When the same parameterization was used in the European Centre for Medium-Range Weather Forecasts (ECMWF) model, Slingo (1987) modified the coefficients of the parameterizations:

$$N = -6.67(\Delta\theta/\Delta p)_{min} - 0.667,$$

$$\text{for } -0.25 \leq (\Delta\theta/\Delta p)_{min} \leq -0.1. \quad (3)$$

For $(\Delta\theta/\Delta p)_{min} > -0.1$, $N = 0$, and for $(\Delta\theta/\Delta p)_{min} < -0.25$, $N = 1$. Equation (3) has not only been used in the ECMWF model but is also the standard for the National Center for Atmospheric Research Community Climate Model Version 2 (NCAR CCM 2) (Kiehl et al. 1994).

Given that low-cloud amount is correlated reasonably well with the stability of the lower troposphere, one might expect a correlation between low-cloud amount and the inversion strength. Figure 9 displays the scatterplot of nighttime low-cloud amount against the inversion strength, which was calculated as the jump in potential temperature across the 50-mb layer identified as the trade inversion (section 2a). Low-cloud amount is reasonably well correlated with inversion strength. In fact, the correlation coefficient between inversion strength and nighttime low-cloud amount is the highest of any presented in this paper. The two solid lines indicate the parameterizations of Slingo (1980) and Slingo (1987) after I set Δp equal to minus 50 mb. The observations generally lie in between the two parameterizations.

c. Betts–Boers mixing line slope

Betts and Boers (1990) suggested that low-cloud amount could be parameterized using the mixing line slope. The mixing line slope measures the relative change with height in the boundary layer of two conservative variables: saturation point potential temperature and saturation point mixing ratio. It is called a "mixing line" because the points in a scatterplot of these two variables tend to lie along a straight line, as air that is the result of conservative mixing would tend to do. The slope of this mixing line, when normalized by the slope of the moist adiabat, is the parameter Betts and Boers used to parameterize low-cloud amount. Their parameterization of cloud amount as a function of the normalized mixing line slope, Γ_m/Γ_w, is

$$N = 0.5 + 3.2(\Gamma_m/\Gamma_w - 0.49),$$

$$\text{for } 0.33 \leq \Gamma_m/\Gamma_w \leq 0.65, \quad (4)$$

where Γ_m is the mixing line slope and Γ_w is the moist adiabat slope. For $\Gamma_m/\Gamma_w < 0.33$, $N = 0$, and for $\Gamma_m/\Gamma_w > 0.65$, $N = 1$. The mixing line slope is related to cloud-top entrainment instability (Randall 1980; Deardorff 1980) such that smaller mixing line slopes are more unstable. In this parameterization, a smaller mixing line slope is assigned a smaller cloud amount.

To numerically test the Betts and Boers parameterization, I follow the procedure of Albrecht et al. (1995b), by defining a stability parameter, σ, which is approximately equal to the normalized mixing line slope, Γ_m/Γ_w:

$$\sigma = \frac{-c_p\Delta\theta}{L\Delta w_T}, \quad (5)$$

where $\Delta\theta$ is the jump in potential temperature across the trade inversion and Δw_T is the jump in total (vapor plus liquid) water mixing ratio across the inversion. Because soundings do not have measurements of liquid water, I evaluate the jump in two ways that bracket the likely values of liquid water mixing ratio. According to the first method, σ is evaluated by using the values of potential temperature and vapor mixing ratio interpolated to inversion normalized heights of 1.15 and 0.9:

$$\sigma = \frac{-c_p[\theta(z/z_i = 1.15) - \theta(z/z_i = 0.9)]}{L[w(z/z_i = 1.15) - w(z/z_i = 0.9)]}. \quad (6)$$

Because setting the total water mixing ratio equal to the vapor mixing ratio at a normalized height of 0.9 assumes no liquid water present in the cloud, this will be called the minimum liquid water assumption. This assumption tends to underestimate the drop in total water at the inversion. The second method is to use boundary layer air properties at a normalized height of 0.2:

$$\sigma = \frac{-c_p[\theta(z/z_i = 1.15) - \theta(z/z_i = 0.2)]}{L[w(z/z_i = 1.15) - w(z/z_i = 0.2)]}. \quad (7)$$

This assumes that cloudy air just beneath the inversion have a total water mixing ratio equal to the generally larger vapor mixing ratio of subcloud air and is equivalent to assuming the maximum possible liquid water in the cloud. This assumption will be called the maximum liquid water assumption and results in the greatest possible drop in total water mixing ratio at the inversion.

For both methods, the observed cloud amount increases with σ (Fig. 10). As expected, the maximum liquid water assumption (Fig. 10b) has lower values of σ and is more unstable with respect to cloud-top entrainment instability. Interestingly, the slope of the smooth curve fits to the data (which are indicated by the dashed lines) are very similar to slope of Betts and Boers parameterization (4), which is indicated in both figures by the solid line. It is interesting to note some of the previous tests of this parameterization against data. Although the original parameterization was based only upon data from a single day during the FIRE experiment (Betts and Boers 1990), the slope of the parameterized line were recently supported by considering the diurnal variation of composite soundings taken by the ship R/V *Valdivia* during the ASTEX experiment (Betts et al. 1995). However, Albrecht et al. (1995b) found that their data from three different field experiments suggested a slope of cloud amount on σ, which was 4 times smaller than the parameterization of Betts and Boers (1990). Our results support the original slope of Betts and Boers (1990); however, the result of Albrecht et al. (1995b) may have more validity since their soundings sample a wider range of conditions. [It is interesting to note that a similar discrepancy holds for the slope of cloud amount on the stability of the lower troposphere. Figure 3b suggests a slope of 0.25 $(^{\circ}C)^{-1}$, whereas consideration of seasonal and interannual variability suggests a slope of near 0.05$(^{\circ}C)^{-1}$ (Klein and Hartmann 1993).]

d. Albrecht's saturation ratio parameterization

One of the more novel parameterizations of cloud amount involves parameterizing the amount of cloud as a function of both the relative humidity of air and the amount of liquid water in the cloud (Albrecht 1981). According to this parameterization, if a certain cloud had a higher liquid water content, it would take longer for that cloud to evaporate into the surrounding clear air than for a cloud with lower liquid water content evaporating into the same air. As a consequence, the cloud with the greater liquid water content would occupy more of the sky while it evaporated. The amount of liquid water in the cloud is measured by the saturation ratio, SR, of cloudy air parcels, which is defined as the ratio of the total (liquid plus vapor) mixing ratio of the cloudy air to the saturation vapor mixing ratio of the cloud-layer environment, w_s. From the SR and the relative humidity RH (as a fraction) of the clear air the
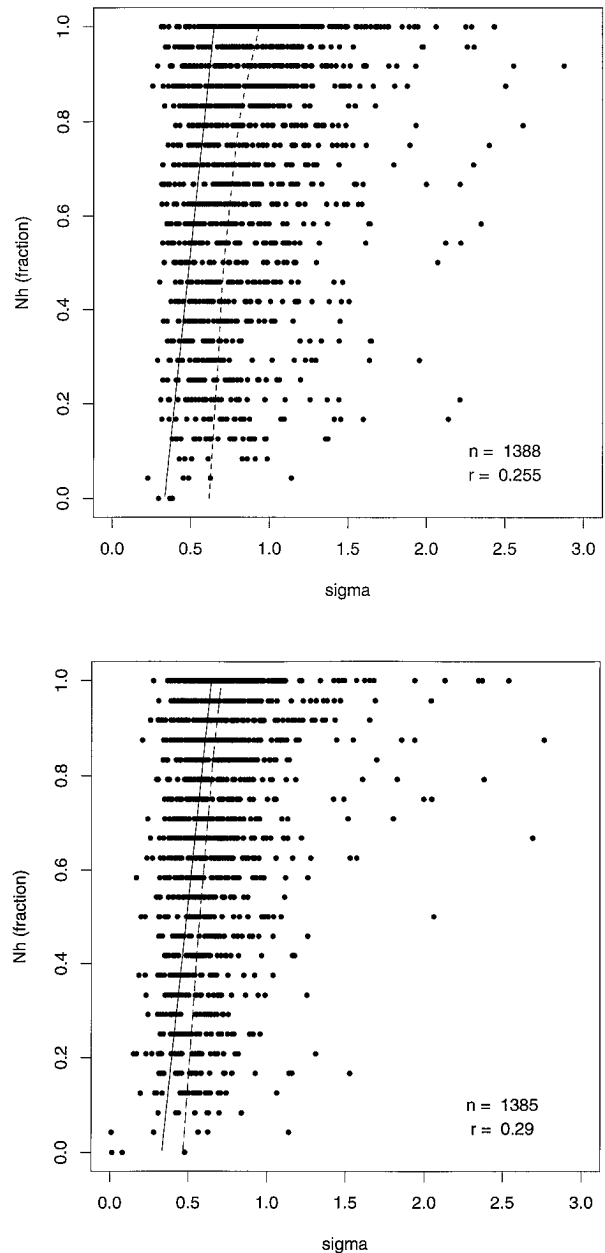

FIG. 10. (a) Scatterplots of Nh against the stability parameter σ. The stability parameter is calculated using boundary layer values under the minimum liquid water assumption. The thin dashed line is the smoothed curve fit to the data. The solid line is the parameterization of cloud amount as a function of the stability parameter by Betts and Boers (1990). (b) As in (a) except the stability parameter is calculated using boundary layer values under the maximum liquid water assumption.

cloud evaporates into, Albrecht (1981) proposed that the trade cumulus cloud amount should be parameterized as

$$N = \frac{SR - 1}{SR - RH}. \qquad (8)$$

Because the soundings do not have measurements of liquid water, the following method of Albrecht et al. (1995b) was used to estimate SR. A simple model for the total water mixing ratio of active updrafts in cumulus clouds is constructed by assuming that the updraft air parcel starts with a total water mixing ratio equal to the average water vapor mixing ratio in the subcloud layer. As the parcel ascends, entrainment dilutes then parcel's total water mixing ratio, w_p, toward the environment's water vapor mixing ratio, w_{env}, according to

$$\frac{dw_p}{dp} = \lambda(w_p - w_{env}), \qquad (9)$$

where λ is an entrainment parameter set equal to 0.004 mb^{-1} (Albrecht 1981). For each sounding in the OWS N record with an identifiable trade inversion, Eq. (9) was integrated from the inversion normalized height of 0.2 to the inversion normalized height of 0.9 with the initial parcel mixing ratio set equal to the water vapor mixing ratio interpolated to the inversion normalized height of 0.2. The SR was then set equal to the parcel's total water mixing ratio after the integration of Eq. (9) divided by the saturation vapor mixing ratio of environmental air at the inversion normalized height of 0.9. The relative humidity of environmental air interpolated to that same height (which is exactly the same as RH_{cl}) was used as the RH in Eq. (8). If the calculated SR was less than one, the calculated cloud amount from Eq. (8) was set equal to zero. This corresponds to the case where the subcloud layer is so dry that air lifted from the subcloud layer would not have enough moisture to be a cloud at the level just beneath the trade inversion.

The scatterplot of the cloud amount calculated with Eq. (8) against the observed cloud amount is shown in Fig. 11a. If Eq. (8) were a perfect parameterization of cloud amount, then all the points would lie along the diagonal solid line. As it is, the smooth curve fit to the data does indicate some rise of observed cloud amount with calculated cloud amount at small values of the cloud amount. At greater values of the observed cloud amount, the calculated cloud amount levels out near 0.6. This results because the typical values of RH_{cl} for overcast conditions is only 90%. At RH = 0.9, Eq. (8) gives a cloud amount of 0.46 for an SR of 1.085 (the median of the calculated SR). Thus the likely underestimate of relative humidity by radiosonde errors or poor vertical resolution hinders an accurate evaluation of the parameterization. If all the relative humidities in the boundary layer are increased by 7.2% (which is the underestimate of relative humidity according to composite sounding in Fig. A3) while keeping all relative humidities less than or equal to 100%, the comparison between calculated and observed cloud amounts improves somewhat (Fig. 11b). In this case, not only has the cloud level relative humidity increased, but the median saturation ratio has
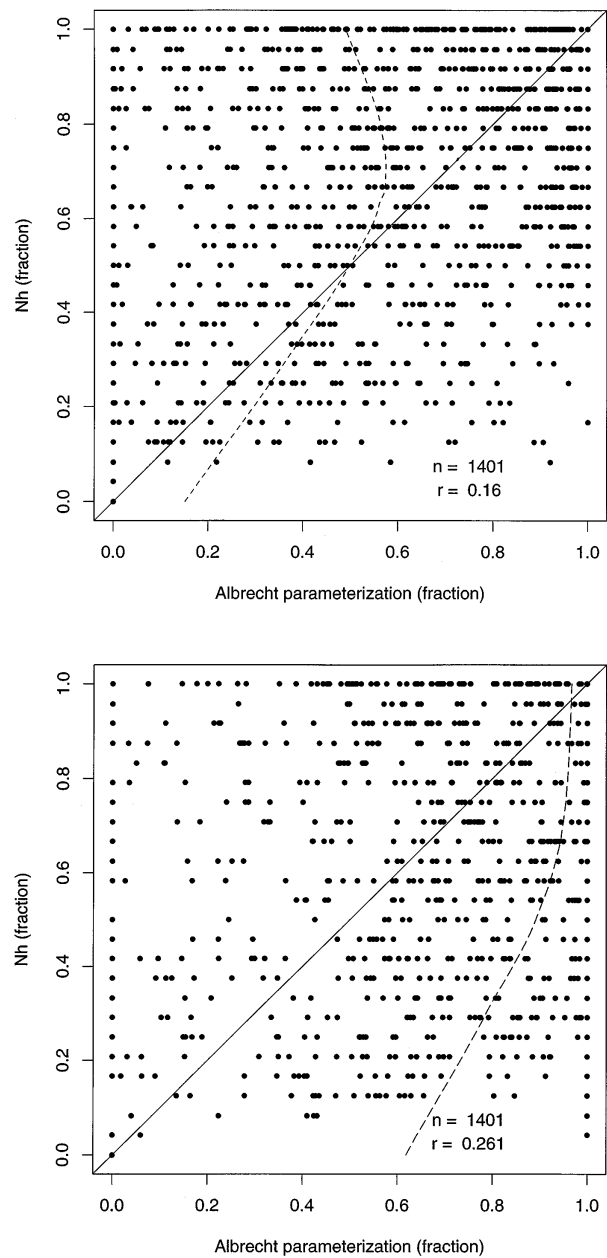

FIG. 11. (a) Scatterplots of Nh against the Albrecht (1981) parameterization of cloud amount. The thin dashed line is the smoothed curve fit to the data. (b) As in (a) except that all relative humidities in the boundary layer have been increased by 7.2%.

increased from 1.085 to 1.175. The calculated cloud amounts now approach one more frequently and the agreement between observation and parameterization improves notably at the higher values of cloud amount. However, this comes at the expense of a poorer estimation at low values of the observed cloud amount. In general, the parameterization of Albrecht (1981) correlates with the observations about as well

Table 4. Correlation coefficients between cloud amounts calculated from several parameterizations and observed nighttime low-cloud amounts. All correlations are significant at the 99% level.

Parameterization	Correlation coefficient
Sundquist relative humidity [Eq. (1)]	0.318
Sundquist relative humidity [Eq. (1)] after all relative humidities have been increased by 7.2%	0.323
Slingo (1980) inversion strength [Eq. (2)]	0.303
Slingo (1987) inversion strength [Eq. (3)]	0.395
Betts and Boers (1990) mixing line slope [Eq. (4)] with minimum liquid water assumption	0.219
Betts and Boers (1990) mixing line slope [Eq. (4)] with maximum liquid water assumption	0.324
Albrecht (1981) saturation ratio [Eq. (8)]	0.160
Albrecht (1981) saturation ratio [Eq. (8)] after all relative humidities have been increased by 7.2%	0.261

as the other parameterizations considered in this study (Table 4).

6. Conclusions and discussion

There are three principal conclusions from this study of sypnoptic variability at a site in the subtropical trade wind boundary layer:

- The relationships between low-cloud amount and the available meteorological parameters are the same at the synoptic timescale as they are at the monthly mean timescale. Namely, increases in the amount of low cloud are associated with increases in cold advection, the stability of the lower troposphere, and the relative humidity just beneath the trade inversion.
- The amount of variance in low-cloud amount that can be explained by the available meteorological parameters is very low. However, if the data are averaged over a few days, the variance explained increases dramatically (Fig. 5).
- Existing diagnostic parameterizations of the amount of low cloud are positively correlated with the observed variations in the amount of low cloud; however, the amount of explained variance is very low.

With regard to physical explanations for the principal relationships, the correlation between temperature advection and low-cloud amount may be explained by the necessity of upward sensible and latent heat fluxes to maintain an elevated cloud under conditions of mean subsidence. The amount of low cloud may be correlated with the stability of the lower troposphere, because increases in stability may indicate increased subsidence, a condition favorable for the occurrence of low cloud. As in KHN, evidence exists that cloudiness is better related to the stability of the lower troposphere when the changes in stability lead the changes in cloudiness

by about 1 day. With regard to the correlation between low-cloud amount and relative humidity, variations in the relative humidity of cloud layer air may result from cloudiness variations and not be the cause of cloudiness variations. The correlation of low-cloud amount with relative humidity reinforces observational results from other cloud types [cirrus: Soden and Bretherton (1993); midlatitude cyclone clouds: Walcek (1994)]. It is also reassuring since both diagnostic and prognostic cloud parameterizations still widely relate cloud cover to the relative humidity of the layer.

Unfortunately no single meteorological parameter explains more than 13% of the variance in nighttime low-cloud amount. Furthermore multiple regression does not dramatically increase the explained variance. This is in sharp contrast to the results of studies using monthly mean data, which show that variations in external factors may explain over 50% of the variance in monthly mean low-cloud amount. The poor correlation does not result because the synoptic variation in cloud amount is small; the standard deviation in nighttime low-cloud amounts is 0.27, whereas the standard deviation of monthly mean cloud amounts is 0.10. The fairly low amount of variance in low-cloud amount that can be explained by any set of predictors is a cause of concern. Here I offer four potential explanations for the inefficiency of the predictors in this study. 1) Other predictors that were not included in this study may explain more variance. Important predictors not included in this study include direct measurements of the large-scale subsidence field or the amount of cloud condensation nuclei, neither of which are available for each individual day. With regard to subsidence (which could only be addressed through compositing), the composite COADS wind fields suggest that subsidence at and upwind from N increases with low-cloud amount. However, I suspect that subsidence would not explain much additional variance in low-cloud amount since variations in subsidence are probably coupled to variations in stability of the lower troposphere and temperature advection, variables already measured. 2) Observational and instrumental error is always possible. The difficulty in ascertaining relative humidity in the upper part of the boundary layer hindered some of the quantitative comparisons of the data. 3) The most important predictors may be nonlocal (KHN). Cloudiness at N may be better related to large-scale factors at earlier times and other (upwind) locations. 4) Random effects may be important. Wyant et al. (1997) demonstrate that the low-cloud amount in an eddy resolving model of the boundary layer at any given instant differs substantially between runs that vary only trivially by initial random seeds. Whether or not randomness can account for substantial variability in nighttime averaged low-cloud amount (or actually the mean over 6 h of three evenly spaced in time point observations of low-cloud amount) is unclear. Of

course, not being able to explain a high fraction of the variance in low-cloud amount at daily timescales may not be distressing if you are more interested in predicting climate anomalies.

With regard to commonly used parameterizations, the data in the paper cautiously support all of the studied parameterizations. The inversion strength parameterization of Slingo [Eq. (3)], which was used in the ECMWF model and the CCM2, appears to do a reasonable job of predicting the cloud amount variations studied in these paper, although the slope from the parameterization is perhaps a bit too small. Problems with the relative humidity measurement in the upper part of the boundary layer hinders however a more precise comparison of the other parameterizations with data.

Finally, the fact that variations only at a single point have been studied means that one should view with caution the results in this paper. The relationships shown here may not apply to other locations. The strong correlation between temperature advection and low-cloud amount at N may result from N being located on the border between a region dominated by trade cumulus, with a small amount of low cloud, and a colder region dominated by stratocumulus, with a larger amount of low cloud. Studies of low-cloud variations in other climatologically important regions (midlatitude oceans, the Arctic Ocean, over land) are desperately needed.

APPENDIX

Corrections to Radiosonde Relative Humidity Data

In this appendix, I discuss the corrections applied to the relative humidity data from the radiosonde record. An analysis of day to night differences in relative humidity at fixed radiosonde pressure levels revealed a sharp discontinuity in the time record near the beginning of 1966 (Klein 1994). The sharp discontinuity is suggestive of a change in the radiosonde instru-

ment. Indeed at the time Teweles (1970) noted that although the new radiosondes used at U.S. stations had a quicker response time in the hygristor element than previous instruments, a spurious decrease in daytime relative humidity occurred. This spurious decrease in daytime relative humidity was attributed to solar heating of the hygristor strip. Klein (1994) detected the same spurious decrease in daytime relative humidity in the record at OWS N, a U.S. weather station. Prior to 1966, the 900-mb relative humidity from the day sounding (0000 UTC or 1440 LT) was typically 3% lower than the relative humidity from the nighttime sounding (1200 UTC or 0240 LT) at the same level. After the beginning of 1966 the daytime relative humidity was 20% lower than the corresponding nighttime relative humidity. For this reason, I did not consider daytime radiosonde records.

Unfortunately, the change in radiosonde instruments introduces changes into the nighttime humidity data as well. Figures A1 and A2 present the histogram of the nighttime relative humidity at the 900-mb level for data taken before and after 1 January 1966. Clearly visible is a shift of the mode relative humidity from 77.5%–85% before 1966 to 90%–92.5% after 1966. I suggest that this change in the frequency distribution of relative humidity represents the effect of the change in instruments and not a real change. One can argue that this increase in the mode relative humidity is consistent with the decrease in response time for the hygristor that occurred with the change in U.S. radiosondes in the late 1960s. Because the response time of the hygristor is finite, the temperature on the hygristor strip is reflective of the temperature of a layer beneath the radiosonde and not the temperature at the level of the radiosonde. In regions where temperature decreases with height (such as the boundary layer), the hygristor temperature will be warmer than the ambient temperature and as a consequence report a lower relative humidity than true relative humidity. For example, if the response time of the hygristor is 30 s (Teweles 1970) and the ascent rate of the radiosonde is 5 m s^{-1} (Teweles 1970), then the temperature of the hygristor strip will be 1.2 K warmer than the ambient temperature if the lapse rate is 8 K/km. If the true temperature and relative humidity at 900 mb are 283 K and 90% respectively, for this error in hygristor temperature the measured temperature and relative humidity will be 284.2 K and 82% relative humidity. Thus a decrease in response time of the hygristor as was known to have occurred with the change in U.S. radiosondes (Teweles 1970) would be consistent with the general increase in 900-mb relative humidity observed at OWS N after 1966.

To correct for the change in radiosonde instruments near 1966, the pre-1966 relative humidities were changed so that the resultant histogram of relative humidities of pre-1966 data would be identical to that of post-1966 data. The correction factors needed to make
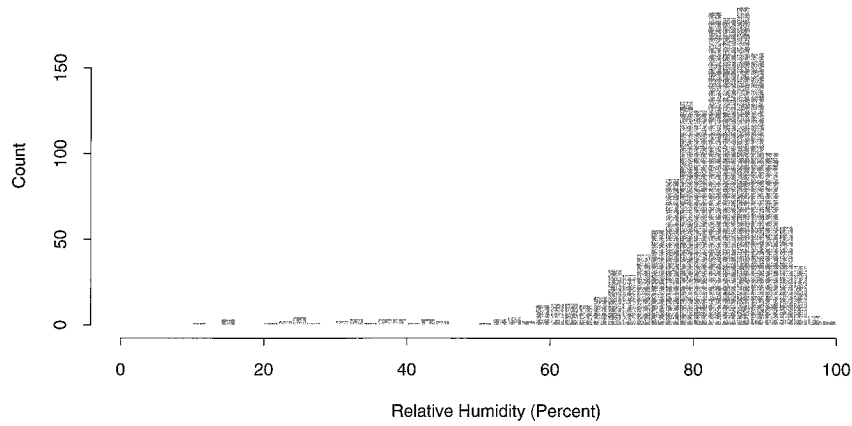
Before 1966

FIG. A1. Histogram of June–September nighttime relative humidities at 900 mb from data before 1 January 1966.

the two histograms identical are shown in Table A1. The corrections at 900 mb were generally consistent with those at other vertical levels except at the surface and 1000 mb where the corrections needed were much smaller in magnitude than at all other levels. Consequently, the correction factors in Table A1 were applied to each sounding before 1966 at all vertical levels except the surface and 1000 mb. The soundings after 1 January 1966 were unaltered.

To illustrate the effect of this correction, the in-version-normalized composite sounding for those surface observations that report a solid overcast under conditions of adequate moonlight was computed for soundings before and after 1 January 1966 and with the uncorrected and corrected data. The result (Fig. A3) shows that the relative humidity in the upper part of the boundary layer increases from 84.5% in the uncorrected pre-1966 data to 89.4% in the corrected pre-1966 ("v1") data. The post-1966 data, which is not affected by this correction, indicates a relative
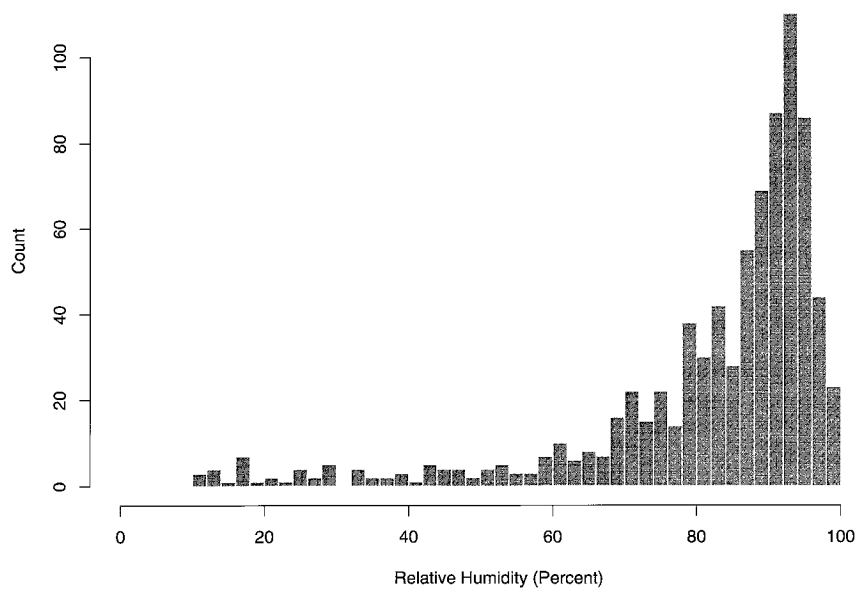
After 1966

FIG. A2. Histogram of June–September nighttime relative humidities at 900 mb from data after 1 January 1966.

TABLE A1. Correction factors added to pre-1966 relative humidities as a function of the uncorrected relative humidity. These correction factors were applied only to data from levels higher in altitude than the 1000-mb level.

Uncorrected relative humidity (%)	Relative humidity correction (%)
0	0.00
5	0.91
10	2.02
15	3.45
20	1.95
25	0.72
30	−0.91
35	−2.28
40	−3.32
45	−3.97
50	−4.10
55	−3.97
60	−3.58
65	−3.38
70	−2.80
75	−1.50
80	1.43
85	5.26
90	5.40
95	5.00
100	0.00

humidity of 89.1% in the upper part of the boundary layer.

The fact that these relative humidities are not that close to 100% despite the report of overcast from the surface observer suggests that even the post-1966 radiosondes have some instrumental error in relative humidity. As noted above, Teweles (1970) suggested that the hygristor strip's temperature in the new U.S. radiosondes had a response time of 30 s, which in regions of temperature decreasing with height could lead to underestimates in relative humidity of 5%–10%. By comparing the hygristor strip temperatures to those taken by an external white thermistor affixed to radiosondes, Morrissey and Brousaides (1970) determined that for U.S. radiosondes the appropriate correction factor to nighttime relative humidities is 1.05 in the 1000–700-mb layer (Table 2 of Teweles 1970). Consequently, as a second correction to the data, I multiplied all relative humidities at levels higher than 1000 mb in the OWS N record by 1.05. Any resulting relative humidities that exceeded 100% were lowered to 100%. [I note that similar corrections have been applied to radiosondes used in modern field experiments (Albrecht et al. 1995b).] The relative humidities in the composited soundings after this second correction (''v2'') was applied are near 92.8% in the upper part of the boundary layer (Fig. A3). This value is still a fair amount below 100%; however, further corrections were not applied to the data because many individual soundings reported 100% relative humidity. A portion of the difference between 92.8% and 100% may be attributed to the poor 50-mb resolution of the original soundings. An analysis of high-resolution soundings taken from the ship R/V *Valdivia* during the ASTEX experiment suggested that when the original sounding with near-5-mb resolution was sampled at 50-mb intervals to match the resolution of the OWS N soundings, the composited relative hu-
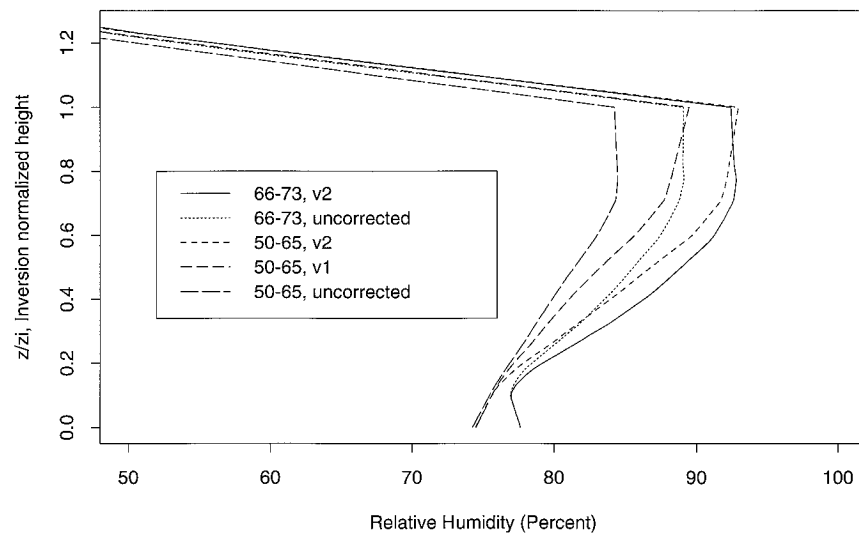

FIG. A3. Inversion-normalized soundings of nighttime relative humidity. The soundings are composited only at hours when the surface observer reports overcast with low clouds under conditions of adequate moonlight. ''Uncorrected'' refers to data before relative humidity corrections were applied, ''v1'' refers to data after which only the first correction was applied, and ''v2'' refers to data after which both the first and second corrections were applied.

midities in the upper part of the boundary layer dropped by 2%–3%.

REFERENCES

Agee, E. M., T. S. Chen, and K. E. Dowell, 1973: A review of mesoscale cellular convection. *Bull. Amer. Meteor. Soc.,* **54,** 1004–1012.

Albrecht, B. A., 1981: Parameterization of trade-cumulus cloud amount. *J. Atmos. Sci.,* **38,** 97–105.

——, D. A. Randall, and S. Nicholls, 1988: Observations of marine stratocumulus during FIRE. *Bull. Amer. Meteor. Soc.,* **69,** 618–626.

——, C. S. Bretherton, D. Johnson, W. Schubert, and A. S. Frisch, 1995a: The Atlantic Stratocumulus Transition Experiment—ASTEX. *Bull. Amer. Meteor. Soc.,* **76,** 889–904.

——, M. Jensen, and W. J. Syrett, 1995b: Marine boundary layer structure and fractional cloudiness. *J. Geophys. Res.,* **100,** 14 209–14 222.

Barrett, E. C., and C. K. Grant, 1979: Relations between frequency distributions of cloud cover over the United Kingdom based on conventional observations and imagery from Landsat 2. *Weather,* **34,** 416–424.

Betts, A. K., 1989: The diurnal variation of California coastal stratocumulus from two days of boundary layer soundings. *Tellus,* **42A,** 302–304.

——, and R. Boers, 1990: A cloudiness transition in a marine boundary layer. *J. Atmos. Sci.,* **47,** 1480–1497.

——, C. S. Bretherton, and E. Klinker, 1995: Relation between mean boundary layer structure and cloudiness at the R/V *Valdivia* during ASTEX. *J. Atmos. Sci.,* **52,** 2752–2762.

Bretherton, C. S., and M. C. Wyant, 1997: Moisture transport, lower-tropospheric stability and decoupling of cloud-topped boundary layers. *J. Atmos. Sci.,* **54,** 148–167.

——, E. Klinker, A. K. Betts, and J. Coakley, 1995: Comparison of ceilometer, satellite, and synoptic measurements of boundary layer cloudiness and the ECMWF diagnostic cloud parameterization scheme during ASTEX. *J. Atmos. Sci.,* **52,** 2736–2751.

Deardorff, J. W., 1980: Cloud top entrainment instability. *J. Atmos. Sci.,* **37,** 131–147.

Dorman, C. E., 1985: Evidence of Kelvin waves in California's marine layer and related eddy generation. *Mon. Wea. Rev.,* **113,** 827–839.

Fu, R., W. T. Liu, and R. E. Dickinson, 1996: Response of tropical clouds to the interannual variation of sea surface temperature. *J. Climate,* **9,** 616–634.

Hahn, C. J., S. G. Warren, and J. London, 1996: Edited synoptic cloud reports from ships and land stations over the globe, 1982–1991. Rep. #NDP026B, 45 pp. [Available from Carbon Dioxide Information Analysis Center, Oak Ridge National Laboratory, P. O. Box 2008, Oak Ridge, TN 37831-6050.]

——, ——, and ——, 1995: The effect of moonlight in observation of cloud cover at night, and application to cloud climatology. *J. Climate,* **8,** 1429–1446.

Hanson, H. P., 1991: Marine stratocumulus climatologies. *Int. J. Climatol.,* **11,** 147–164.

Heck, P. W., B. J. Byars, D. F. Young, P. Minnis, and E. Harrison, 1990: A climatology of satellite-derived cloud properties over marine stratocumulus regions. Preprints, *Conf. on Cloud Physics,* San Francisco, CA, Amer. Meteor. Soc., J1–J7.

Henderson-Sellers, A., M. Desbois, F. Drake, and G. Sèze, 1987: Surface-observed and satellite retrieved cloudiness compared for the 1983 ISCCP special study area in Europe. *J. Geophys. Res.,* **92,** 4019–4033.

Kiehl, J. T., J. J. Hack, and B. P. Briegleb, 1994: The simulated Earth radiation budget of the National Center from Atmospheric Research community climate model CCM2 and com-

parisons with the Earth Radiation Budget Experiment (ERBE). *J. Geophys. Res.,* **99,** 20 815–20 827.

Klein, S. A., 1994: Large-scale variations in boundary layer cloud cover and their relationships to meteorological parameters. Ph.D. dissertation, University of Washington, 206 pp. [Available from Dept. of Atmospheric Sciences, Box 351640, University of Washington, Seattle, WA 98195-1640.]

——, and D. L. Hartmann, 1993: The seasonal cycle of low stratiform clouds. *J. Climate,* **6,** 1587–1606.

——, ——, and J. R. Norris, 1995: On the relationships among low-cloud structure, sea surface temperature, and atmospheric circulation in the summertime northeast Pacific. *J. Climate,* **8,** 1140–1155.

Kloesel, K. A., 1992: Marine stratocumulus cloud clearing episodes observed during FIRE. *Mon. Wea. Rev.,* **120,** 565–578.

Krueger, S. K., G. T. McLean, and Q. Fu, 1995a: Numerical simulation of the stratus-to-cumulus transition in the subtropical marine boundary layer. Part I: Boundary-layer structure. *J. Atmos. Sci.,* **52,** 2839–2850.

——, ——, and ——, 1995b: Numerical simulation of the stratus-to-cumulus transition in the subtropical marine buondary layer. Part II: Boundary-layer circulation. *J. Atmos. Sci.,* **52,** 2851–2868.

Leipper, D. F., 1994: Fog on the U.S. west coast. *Bull. Amer. Meteor. Soc.,* **75,** 229–240.

Leith, C. E., 1973: The standard error of time-average estimates of climatic means. *J. Appl. Meteor.,* **12,** 1066–1069.

Mass, C. F., and M. D. Albright, 1989: Origin of the Catalina eddy. *Mon. Wea. Rev.,* **117,** 2406–2436.

Minnis, P., and E. F. Harrison, 1984: Diurnal variability of regional cloud and clear-sky radiative parameters derived from GOES data. Part II: November 1978 cloud distributions. *J. Climate Appl. Meteor.,* **23,** 1012–1031.

——, P. W. Heck, D. F. Young, C. W. Fairall, and J. B. Snider, 1992: Stratocumulus cloud properties derived from simultaneous satellite and island-based instrumentation during FIRE. *J. Appl. Meteor.,* **31,** 317–339.

Morrissey, J., and F. J. Brousaides, 1970: Temperature-induced errors in the ML-476 humidity data. *J. Appl. Meteor.,* **9,** 805–808.

Nicholls, S., 1984: The dynamics of stratocumulus: Aircraft observations and comparisons with a mixed layer model. *Quart. J. Roy. Meteor. Soc.,* **110,** 783–820.

Norris, J. R., and C. B. Leovy, 1994: Interannual variability in stratiform cloudiness and sea surface temperature. *J. Climate,* **7,** 1915–1925.

Oreopoulos, L., and R. Davies, 1993: Statistical dependence of the albedo and cloud cover of tropical marine stratocumulus on sea surface temperature. *J. Climate,* **6,** 2434–2447.

Paluch, I. R., D. H. Lenschow, J. G. Hudson, and R. Pearson Jr., 1992: Transport and mixing in the lower troposphere over the ocean. *J. Geophys. Res.,* **97,** 7527–7541.

Peterson, T. C., T. P. Barnett, E. Roeckner, and T. H. Vonder Haar, 1992: An analysis of the relationship between cloud anomalies and sea surface temperature anomalies in a global circulation model. *J. Geophys. Res.,* **97,** 20 497–20 506.

Philander, S. G. H., D. Gu, D. Halpern, G. Lambert, N.-C. Lau, T. Li, and R. C. Pacanowski, 1996: Why the ITCZ is mostly north of the equator. *J. Climate,* **9,** 2958–2972.

Quayle, R., 1980: Climatic comparisons of estimated and measured winds from ships. *J. Appl. Meteor.,* **19,** 142–156.

Randall, D. A., 1980: Conditional instability of the first kind upside-down. *J. Atmos. Sci.,* **37,** 125–130.

Rogerson, A. M., and R. M. Samuelson, 1995: Synoptic forcing of coastal-trapped disturbances in the marine atmospheric boundary layer. *J. Atmos. Sci.,* **52,** 2025–2040.

Ronca, R. E., and D. S. Battisti, 1997: Anomalous sea surface temperatures and local air–sea energy exchange on intraannual timescales in the northeastern subtropical Pacific. *J. Climate,* **10,** 102–117.

Rozendaal, M. A., C. B. Leovy, and S. A. Klein, 1995: An observational study of diurnal variations of marine stratiform cloud. *J. Climate,* **8,** 1795–1809.

Slingo, J. M., 1980: A cloud parametrization scheme derived from GATE data for use with a numerical model. *Quart. J. Roy. Meteor. Soc.,* **106,** 747–770.

——, 1987: The development and verification of a cloud prediction scheme for the ECMWF model. *Quart. J. Roy. Meteor. Soc.,* **113,** 899–927.

Smith, S. D., 1988: Coefficients for sea surface wind stress, heat flux, and wind profiles as a function of wind speed and temperature. *J. Geophys. Res.,* **93,** 15 467–15 472.

Soden, B. J., and F. P. Bretherton, 1993: Upper tropospheric relative humidity from the GOES 6.7 μm channel: Method and climatology for July 1987. *J. Geophys. Res.,* **98,** 16 669–16 688.

Sundquist, H., 1978: A parameterization scheme for non-convective condensation including predication of cloud water content. *Quart. J. Roy. Meteor. Soc.,* **104,** 677–690.

Teweles, S., 1970: A spurious diurnal variation in radiosonde humidity records. *Bull. Amer. Meteor. Soc.,* **51,** 836–840.

Walcek, C. J., 1994: Cloud cover and its relationship to relative humidity during a springtime midlatitude cyclone. *Mon. Wea. Rev.,* **122,** 1021–1035.

Wang, S., B. A. Albrecht, and P. Minnis, 1993: A regional simulation of marine boundary layer clouds. *J. Atmos. Sci.,* **50,** 4022–4043.

Weare, B., 1994: Interrelationships between cloud properties and SSTs on seasonal and interannual time scales. *J. Climate,* **7,** 248–260.

Woodruff, S. D., R. J. Slutz, R. L. Jenne, and P. M. Steurer, 1987: A Comprehensive Ocean–Atmosphere Data Set. *Bull. Amer. Meteor. Soc.,* **68,** 1239–1250.

Wyant, M. C., C. Bretherton, H. Rand, and D. Stevens, 1997: Numerical simulations and a conceptual model of the stratocumulus to trade cumulus transition. *J. Atmos. Sci.,* **54,** 168–192.

Wylie, D., B. Hinton, and K. Kloesel, 1989: The relationship of marine stratus to wind and temperature advection. *Mon. Wea. Rev.,* **117,** 2620–2625.